

Oscillations in meta-generalized-gradient approximation potential energy surfaces for dispersion-bound complexes

Erin R. Johnson, Axel D. Becke, C. David Sherrill, and Gino A. DiLabio

Citation: *J. Chem. Phys.* **131**, 034111 (2009); doi: 10.1063/1.3177061

View online: <http://dx.doi.org/10.1063/1.3177061>

View Table of Contents: <http://jcp.aip.org/resource/1/JCPSA6/v131/i3>

Published by the [American Institute of Physics](http://www.aip.org).

Additional information on *J. Chem. Phys.*

Journal Homepage: <http://jcp.aip.org/>

Journal Information: http://jcp.aip.org/about/about_the_journal

Top downloads: http://jcp.aip.org/features/most_downloaded

Information for Authors: <http://jcp.aip.org/authors>

ADVERTISEMENT

physicstoday

Comment on any
Physics Today article.

Physics Today / Volume 65 / July 2012, page 10
Previous Article | Next Article
Measured energy in Japan
David von Seggern
(vonseg@seismo.unr.edu) University of Nevada
July 2012, page 10
DIGITAL OBJECT IDENTIFIER
<http://dx.doi.org/10.1063/PT.3.1619>
The article by Thorne Lay and Hiroo Kanamori is an interesting one. It discusses the energy released by the 2011 Tohoku earthquake. While that of a 100-megaton nuclear device is approximately five times as much energy as that of a 100-megaton atmospheric explosion, the 2011 Chilean earthquake had still more energy by a factor of about 3 or 4. The authors used the relation for seismic energy release rather than total strain energy release. I believe the authors used the relation for seismic energy release by a variable that depends on friction on the fault plane. Accounting for total strain energy release would increase the earthquake energy number by orders of magnitude. Despite the catastrophic damage potential of nuclear bombs, the forces of nature occasionally unleash much larger energy releases. Although the nuclear bombs are under our control, earthquakes, volcanic eruptions, and extreme weather events are not. However, by judicious preparation and avoidance measures, humans can significantly diminish the damage of natural events.
This article does not have any references.
Comment on this article
By the act of hitting a ball with a bat, one calculates the force energy to deliver the ball to its new location, but one must also take into account that the ball extended its energy release to that which became struck by the ball as its momentum ceased and passed energy to the struck team. Therefore the parameters of the damage extend into the future when the received energy to that pushed upon later becomes released in a new event. Perhaps calculations of one added that in while another's calculations did not. E.M.C.
Written by Edgar McCarvill, 14 July 2012 19:59

Oscillations in meta-generalized-gradient approximation potential energy surfaces for dispersion-bound complexes

Erin R. Johnson,¹ Axel D. Becke,² C. David Sherrill,³ and Gino A. DiLabio^{4,a)}

¹Department of Chemistry, Duke University, Durham, North Carolina 27708, USA

²Department of Chemistry, Dalhousie University, Halifax, Nova Scotia B3H 4J3, Canada

³School of Chemistry and Biochemistry, Georgia Institute of Technology, 901 Atlantic Drive NW, Atlanta, Georgia 30332-0400, USA

⁴National Institute for Nanotechnology, National Research Council of Canada, 11421 Saskatchewan Drive, Edmonton, Alberta T6G 2M9, Canada

(Received 14 April 2009; accepted 24 June 2009; published online 17 July 2009)

Meta-generalized-gradient approximations (meta-GGAs) in density-functional theory are exchange-correlation functionals whose integrands depend on local density, density gradient, and also the *kinetic-energy* density. It has been pointed out by Johnson *et al.* [Chem. Phys. Lett. **394**, 334 (2004)] that meta-GGA potential energy curves in dispersion-bound complexes are susceptible to spurious oscillations unless very large integration grids are used. This grid sensitivity originates from the saddle-point region of the density near the intermonomer midpoint. Various dimensionless ratios involving the kinetic-energy density, found in typical meta-GGAs, may be ill-behaved in this region. Grid sensitivity thus arises if the midpoint region is sampled by too sparse a grid. For most meta-GGAs, standard grids do not suffice. Care must be taken to avoid this problem when using, or constructing, meta-GGAs. © 2009 American Institute of Physics.

[DOI: 10.1063/1.3177061]

I. INTRODUCTION

Accurate modeling of the London dispersion interaction using density-functional theory is a challenging problem that has attracted the interest of many researchers. The most popular density functionals, widely used for thermochemistry calculations, completely neglect dispersion. In a study involving 25 functionals, including generalized-gradient approximations (GGAs), meta-GGAs, and hybrids, we showed that none of the methods considered are capable of correctly modeling dispersion-bound complexes.¹ For the benzene dimer, all of the functionals gave potential energy curves that are repulsive at long-range, rather than the correct $1/R^6$ attraction characteristic of dispersion.²

In *ab initio* wave function theory, exact (Hartree–Fock) exchange gives entirely repulsive potential energy curves for dispersion-bound complexes. Dispersion binding is a consequence of electron correlation, arising from instantaneous dipole moments in the electron density.² Thus, dispersion is a dynamical correlation effect that can be modeled by including a large number of high-energy excited state configurations, as in configuration interaction or coupled-cluster theory.

Some GGA-type density functionals give “dispersion-like” binding near minimum-energy separations.^{1,3} However, this binding has been shown to be an artifactual exchange effect^{4,5} and is directly related to the asymptotic behavior of the exchange enhancement factor^{4,6} in the high reduced-density-gradient limit. Functionals such as B88 (Ref. 7) with

a very high asymptotic enhancement factor give potential energy surfaces (PESs) that are excessively repulsive. Conversely, functionals with a low asymptotic enhancement factor, such as PBE,⁸ give some binding. This binding is in a sense spurious since dispersion is properly a correlation effect. It has also been shown that popular correlation functionals do not have the correct dispersion physics built into them.⁹

Several nonempirical approaches to modeling dispersion within a density-functional theory framework have recently been developed. These include the exchange-hole dipole model of Becke and Johnson¹⁰ and functionals based on the nonlocal dispersion model of Andersson *et al.*¹¹ involving interacting uniform-electron-gas regions. Other approaches include addition of empirical dispersion corrections¹² and use of long-range, effective-core-like potentials parameterized to reproduce dispersion binding.¹³

Others¹⁴ have applied meta-GGA functionals to van der Waals complexes and obtained low mean absolute errors for binding energies at equilibrium geometries.¹⁵ Meta-GGA functionals depend on the local kinetic-energy density in addition to the electron density and its gradient. Unlike the density and gradient, inclusion of the kinetic-energy density can introduce some nonlocal information to the functional. For example, when averaged over atomic basins, the ratio of the kinetic-energy density to its uniform-electron-gas analog has been used as an indicator of multicenter delocalization.¹⁶ Thus, there may be a physical basis for meta-GGAs to provide an improved treatment of nonlocal interactions, such as dispersion. However, we found that the meta-GGAs used in our previous study, including TPSS,¹⁷ VSXC,¹⁸ BB95,¹⁹ and B1B95,^{19,20} offered no improvement over GGA functionals

^{a)}Author to whom correspondence should be addressed. Electronic mail: gino.dilabio@nrc.ca.

for dispersion binding.¹ An unsettling sensitivity of meta-GGAs to the size of the integration grid was also revealed. PESs computed using these functionals show large spurious oscillations when using standard integration grids.

One problem associated with oscillations in the PESs is that geometry optimizations can get trapped in one of the many local minima. In order to compute smooth PESs, very large integration grids are required. Meta-GGAs, in particular M06 and M06-L,^{15,21} can also give imaginary frequencies for rotational modes unless extremely large integration grids are used.²² Increasing the numbers of both radial and angular grid points significantly increases the computational expense of the calculations.

In the present work, we extend our study of the suitability of meta-GGAs for modeling dispersion binding to include BMK (Ref. 23) and the M05 (Ref. 24) and M06^{15,21,25} suites of functionals. It will be shown that none of these functionals provide a correct description of dispersion physics. We also unveil the origins of the spurious oscillations in PESs obtained with meta-GGA functionals.

II. THEORETICAL METHODS

Calculations were performed on a set of five dispersion-bound complexes, consisting of the homonuclear dimers of helium, neon, argon, and krypton, as well as the “parallel” or “sandwich” orientation of the benzene dimer (D_{6h} symmetry). The electronic energies of these dimers were evaluated with the aug-cc-pVTZ basis set using ten density functionals: B1B95,^{19,20} BMK,²³ TPSS,¹⁷ and VSXC (Ref. 18) implemented in GAUSSIAN03,²⁶ and M05,²⁴ M05-2X,²⁴ M06,¹⁵ M06-2X,¹⁵ M06-HF,²⁵ and M06-L (Ref. 21) implemented in NWChem.²⁷

In all cases, PESs for the complexes were generated by incrementing the center-of-mass separations in 0.1 Å steps, and subtracting the total energies from those of the infinitely separated monomers. In the case of the benzene dimer, the monomer coordinates were fixed at the geometry of Ref. 28.

The PESs were obtained with integration grids of varying sizes. The notation (n_r, n_ℓ) is used to indicate the grid size, where n_r is the number of radial points per atom and n_ℓ is the number of angular points. In all cases, Lebedev angular grids were used and the grids were chosen to correspond with the default pruned (75,302) grid in GAUSSIAN03, the pruned, ultrafine (99, 590) grid in GAUSSIAN03 (grid=ultrafine), and an even finer, unpruned (250, 590) grid (grid=250,590). These are the same three integration grids considered in our previous work.¹ To allow a more balanced comparison with the GAUSSIAN03 results, the atomic partitioning scheme of Stratmann *et al.*²⁹ was used for all NWChem calculations.

III. RESULTS AND DISCUSSION

A. Incorrect description of dispersion physics

In this section, we assess the abilities of meta-GGA functionals to predict accurate PESs for dispersion-bound complexes. We begin by considering the noble gas pairs. As a representative example, PESs obtained with each of the meta-GGA functionals are shown in Fig. 1 for the argon

dimer. Figure 1 also displays an accurate reference potential for the argon dimer obtained from Ref. 30. The calculated binding energies for all four noble-gas dimers are collected in Table I, along with precise experimental data.³⁰ The (250, 590) grid was used for these calculations. The sensitivity of the calculated PESs to the integration grid size will be discussed in detail in the following section.

For noble gas interactions, the magnitude of dispersion binding is known to increase down the periodic table, following the trend of increasing atomic polarizability. This is reflected in the experimental binding energies. The calculated results show that none of the functionals considered give reasonable binding energy predictions across the entire test set. VSXC gives the correct trend of increasing binding energies along the He₂, Ne₂, Ar₂, Kr₂ series, but drastically overestimates the binding energies themselves, consistent with our previous findings.¹ B1B95 and BMK predict repulsive PESs and no binding. In the case of B1B95, the exchange functional is comprised of a mixing of B88 and HF exchange. Both of these are well known to give entirely repulsive PESs.^{1,3,4,31} The form of the BMK exchange functional resembles B97 (Ref. 32) and HCTH,³³ which are capable of giving either repulsive or attractive PESs (Ref. 1) depending on how the parameterization affects their asymptotic behavior.⁴ M05, M05-2X, and M06-HF predict the correct trend in the noble-gas dimer binding energies, but display insufficient increases in binding with increasing atomic mass. The remaining meta-GGA functionals predict roughly constant binding energies for the four noble-gas dimers. Also, analysis of Fig. 1 reveals that the various bound potential energy curves approach the dissociation limit much more rapidly than the reference potential, which has the correct $-1/R^6$ decay representative of dispersion binding. Thus, the results shown in Table I and Fig. 1 indicate that none of the functionals include the correct physics of the dispersion interaction.

We also calculated PESs for the sandwich or parallel orientation of the benzene dimer, which we previously found to be a particularly challenging case for density functionals.¹ Results obtained with the pruned (99, 590) grid are shown in Fig. 2. Note that the BMK potential has a metastable minimum. This is not a spurious oscillation and the appearance of this feature does not depend on the integration grid size. Spurious oscillations in the calculated PESs will be discussed in the next section. An estimated CCSD(T)/CBS reference curve is also shown for comparison.²⁸ The VSXC curve is omitted from the figure due to its tendency to extremely overbind. VSXC predicts a minimum with binding energy 13.04 kcal/mol, compared to the CCSD(T) binding energy of 1.70 kcal/mol.²⁸ All of the functionals (including VSXC) predict repulsive PESs at long range, whether or not they give dispersion-like binding around the CCSD(T) minimum. This again shows that none of the functionals include correct dispersion physics.

B. Oscillations in PESs

In our previous study of dispersion-bound complexes,¹ meta-GGA functionals were found to be quite sensitive to the

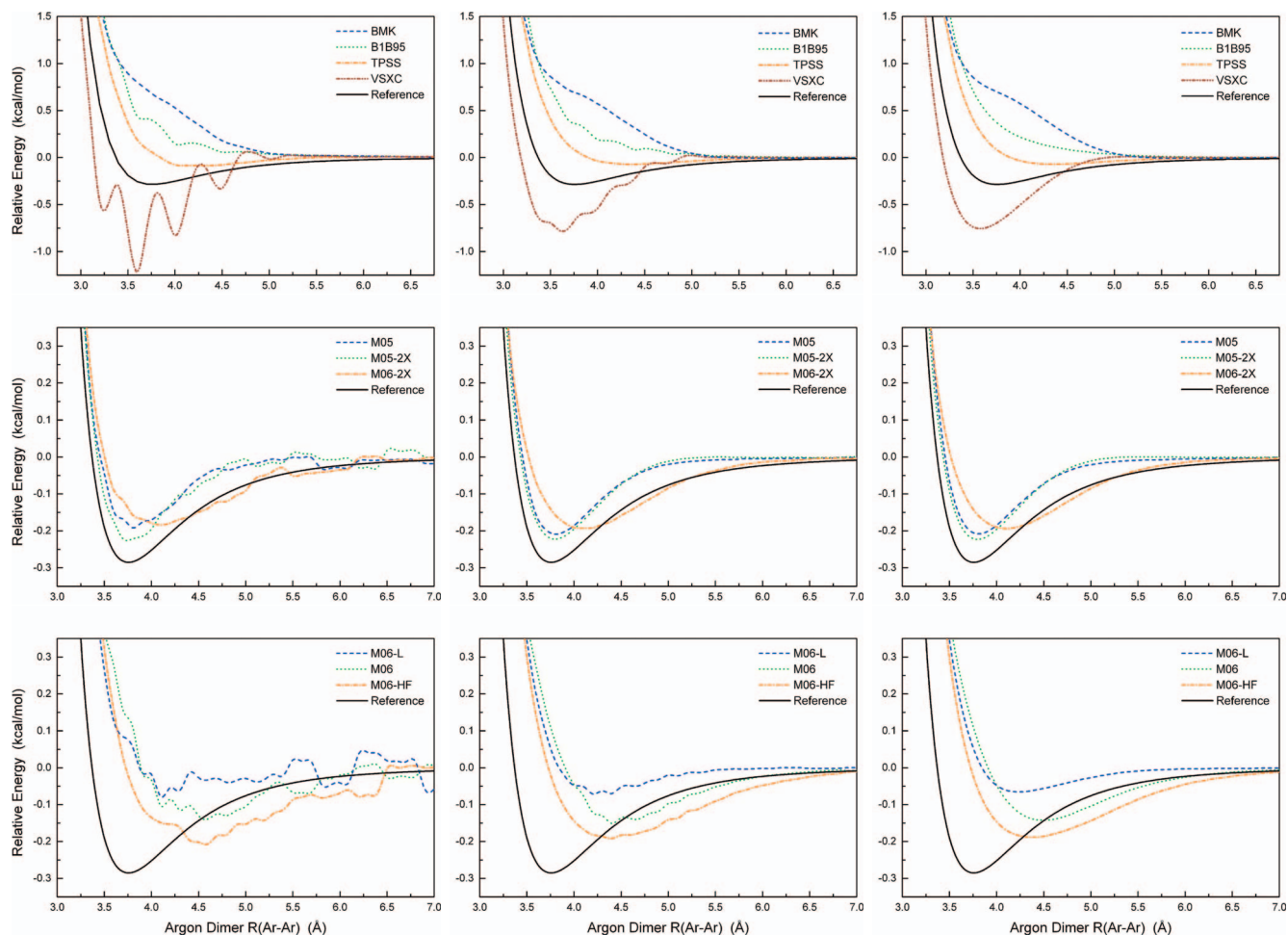


FIG. 1. Potential energy curves for the argon dimer calculated using the $(n_r, n_\ell) = (75, 302)$, $(99, 590)$, and $(250, 590)$ integration grids. The curves on the left are for the coarsest grid and the curves on the right are for the finest grid. The accurate reference potential was obtained from Ref. 30.

choice of integration grid and gave oscillatory PESs unless extremely large integration grids were employed. Similar results are seen in this work for most of the meta-GGA functionals considered. For the noble-gas pairs, use of the default pruned $(75, 302)$ integration grid results in all of the meta-GGAs giving oscillatory PESs, with the exception of TPSS and BMK for some of the dimers. Results are shown for the argon dimer in Fig. 1. Increasing the grid size to ultrafine

$(99, 590)$ results in smooth PESs with BMK, M05, M05-2X, M06-2X, and TPSS. However, B1B95, M06, M06-HF, M06-L, and VSXC still give oscillatory PESs that become smooth upon further increases in grid size. Oscillating PESs are obtained with these same five functionals for the benzene dimer using the $(99, 590)$ grid, as in Fig. 2.

In this section, we aim to understand the sensitivity of meta-GGAs to grid size. To this end, we consider the terms

TABLE I. Calculated binding energies, in kcal/mol, of the noble-gas dimers with 10 meta-GGA density functionals. The mean absolute percent error (MAPE), relative to experiment, (Ref. 30) is also shown.

Method	He ₂	Ne ₂	Ar ₂	Kr ₂	MAPE
Expt. ^a	0.022	0.084	0.285	0.400	...
B1B95	^b	^b	^b	^b	...
BMK	^b	^b	^b	^b	...
M05	0.085	0.206	0.208	0.250	124.3
M05-2X	0.018	0.166	0.223	0.255	43.6
M06	0.120	0.148	0.142	0.156	158.8
M06-2X	0.114	0.192	0.194	0.197	158.2
M06-HF	0.112	0.179	0.188	0.255	139.4
M06-L	0.021	0.143	0.065	0.067	58.6
TPSS	0.048	0.082	0.070	0.073	70.4
VSXC	0.140	0.207	0.754	1.070	254.8

^aReference 30.

^bThe complex is predicted to be unbound.

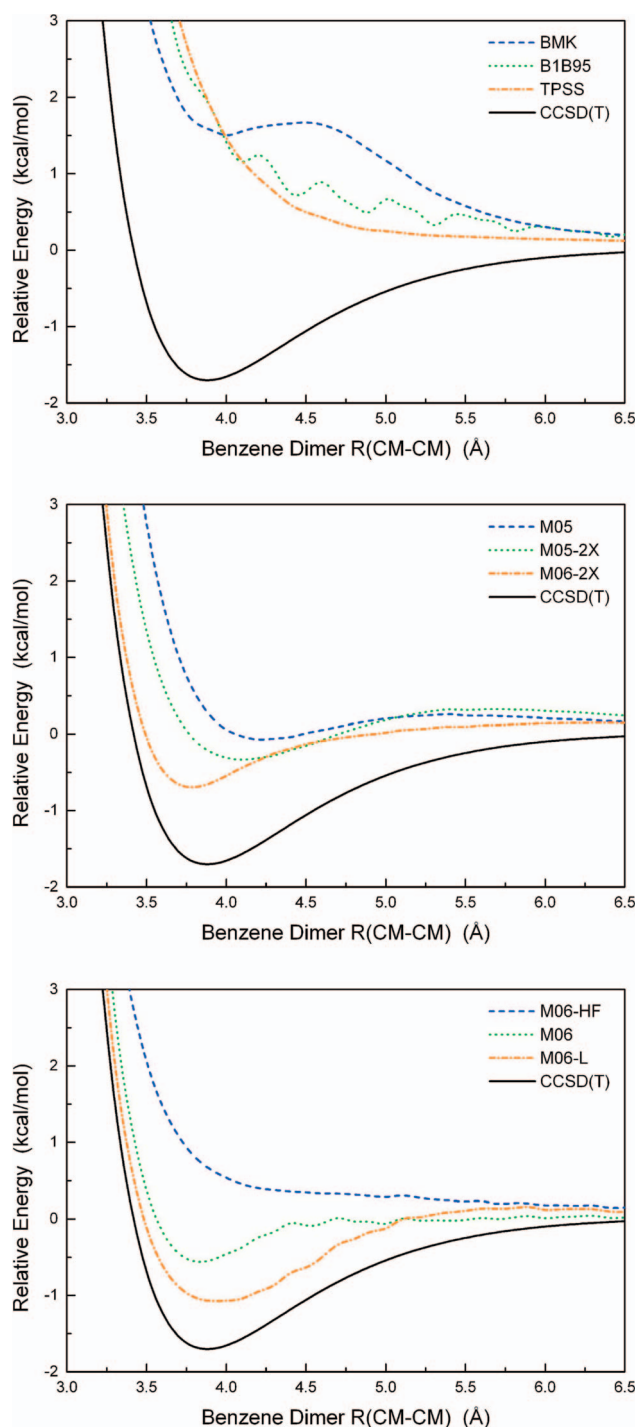


FIG. 2. Potential energy curves for the “sandwich” structure of benzene dimer calculated using the $(n_r, n_\ell) = (99, 590)$ integration grid. VSXC gives a minimum with $BE = 13.04$ kcal/mol at $R = 3.4$ Å (not shown). The CCSD(T) results are from Ref. 28. CM indicates the ring center-of-mass.

in each of the meta-GGA functionals that depend on the kinetic-energy density, and how they behave near the midpoint of dispersion-bound complexes. The rapid variation in some meta-GGA functionals at the midpoint of stretched covalent bonds has been noted previously.³⁴

We begin with B1B95, which has the simplest functional form. The exchange part of B1B95 is comprised of Hartree–Fock and B88 exchange. The observed oscillations in the PESs do not arise from the exchange part because neither HF

nor B88 give oscillating potentials.^{1,3,31} Also, the opposite-spin correlation term in B1B95 (not shown) gives smooth, nonoscillating PESs. The origin of the oscillations in the B1B95 potentials is the parallel-spin correlation term. This is the only component of the functional that depends on the kinetic-energy density. The parallel-spin correlation term of B1B95 has the following form:

$$E_{C\sigma\sigma}^{B95} = \int (1 + 0.038\chi_\sigma^2)^{-2} \frac{D_\sigma}{D_\sigma^{\text{UEG}}} \varepsilon_{C\sigma\sigma}^{\text{UEG}} d\mathbf{r}. \quad (1)$$

In this equation, $\varepsilon_{C\sigma\sigma}^{\text{UEG}}$ is the parallel-spin component of the uniform-electron-gas correlation energy density³⁵ and χ_σ is the reduced spin-density gradient,

$$\chi_\sigma = \frac{|\nabla\rho_\sigma|}{\rho_\sigma^{4/3}}, \quad (2)$$

where ρ_σ is the σ -spin electron density.

The kinetic-energy dependence is in the D_σ term, given by

$$D_\sigma = \tau_\sigma - \tau_\sigma^W, \quad (3)$$

where τ_σ is the σ -spin, positive-definite kinetic-energy density, defined in terms of the Kohn–Sham orbitals by

$$\tau_\sigma = \sum_i |\nabla\psi_{i\sigma}|^2, \quad (4)$$

and τ_σ^W is the Weizsäcker kinetic-energy density,

$$\tau_\sigma^W = \frac{1}{4} \frac{|\nabla\rho_\sigma|^2}{\rho_\sigma}. \quad (5)$$

D_σ vanishes identically in any one-electron system and in many-electron systems it always has positive, nonzero value. As such, it is commonly used to introduce a self-interaction correction into correlation functionals. In the B95 correlation functional, the uniform-electron-gas energy density is corrected for self-interaction by multiplying by D_σ and dividing by its uniform-electron-gas limit, D_σ^{UEG} ,

$$D_\sigma^{\text{UEG}} = \frac{3}{5} (6\pi^2)^{2/3} \rho_\sigma^{5/3}. \quad (6)$$

The behavior of the τ -dependent factor in the B1B95 parallel-spin correlation functional (i.e., the $D_\sigma/D_\sigma^{\text{UEG}}$ ratio) is shown in Fig. 3 for the argon dimer at its experimental equilibrium separation. The plot shows the value of this ratio for grid points along the internuclear axis. The results were obtained from post-LSDA (local spin-density approximation)³⁷ calculations with 160 radial grid points per atom using the NUMOL program.³⁶

The plot of $D_\sigma/D_\sigma^{\text{UEG}}$ in Fig. 3 is highly structured. This ratio is also the key quantity in the electron localization function (ELF) of Becke and Edgecombe.³⁸ Thus, the regions immediately around the nuclei, at ± 1.88 Å, show atomic shell structure. Asymptotically, the ratio approaches infinity for most atoms (including argon), but approaches zero in cases where the angular momentum quantum number $\ell = 0$ for the highest occupied molecular orbital.

We see in Fig. 3, however, that the $D_\sigma/D_\sigma^{\text{UEG}}$ factor in the B95 correlation functional diverges at the midpoint of the argon dimer (at $x = 0$ in the plot). The cause is evident from

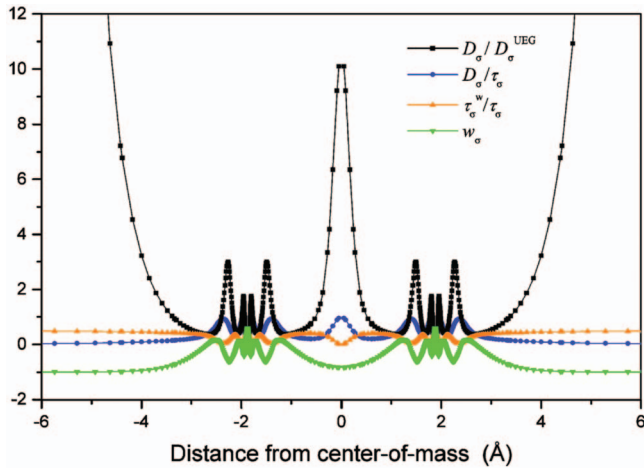


FIG. 3. Plot of the τ -dependent terms in the integrands of the B95 ($D_\sigma/D_\sigma^{\text{UEG}}$), M05 (D_σ/τ_σ), TPSS ($\tau_\sigma^W/\tau_\sigma$), and BMK [$w_\sigma=(D_\sigma^{\text{UEG}}-\tau_\sigma)/(D_\sigma^{\text{UEG}}+\tau_\sigma)$] functionals at grid points along the internuclear coordinate of the argon dimer at its experimental equilibrium geometry ($R=3.76$ Å). The results were obtained from post-LSDA calculations (Ref. 36) using 160 radial grid points per atom, and are given in atomic units.

the functional form. At the midpoint, $\nabla\rho_\sigma=0$, the Weizsäcker term in D_σ vanishes, and the numerator becomes τ_σ . In dispersion-bound complexes, the electron density is extremely small at the midpoint. The τ_σ term in the numerator approaches zero with the same order as ρ_σ , while the D_σ^{UEG} term in the denominator approaches zero more rapidly as $\rho_\sigma^{5/3}$. This leads to divergent behavior in the limit of infinite separation.

This divergence would not be problematic if it were consistently described at all intermonomer separations. However, the use of atom-centered grids means that the placement of integration grid points near the dimer midpoint varies uncontrollably as the dimer is stretched. Moreover, the integration weights in this region are relatively large and their distribution sparse. This means that the energy contribution from grid points near the midpoint can differ greatly at successive increments in the intermonomer separation, resulting in oscillations in the calculated potentials.

The divergence in the τ -dependent parallel-spin correlation term at the midpoint of dispersion-bound dimers clearly explains the observed sensitivity of computed B1B95 PESs to the integration grid size. Oscillations disappear when sufficiently fine grids are used to provide more uniform coverage of the intermonomer region. Oscillations are absent from PESs of hydrogen-bonded complexes, where the density values between monomers are substantially larger than in dispersion-bound complexes.

With this explanation in mind, we now examine the τ -dependence of the other meta-GGA functionals. The M05 form, which is shared by M05-2X, is quite similar to B95. Both involve the kinetic-energy density only in the parallel-spin correlation term. In developing M05, Zhao *et al.*²⁴ also recognized the problems with divergence of the B95 correlation energy and chose to use a modified functional form suggested by Becke.³⁹ This form replaces the $D_\sigma/D_\sigma^{\text{UEG}}$ ratio used in B95 with another dimensionless ratio, D_σ/τ_σ

$$E_{C\sigma\sigma}^{\text{M05}} = \int g_{\sigma\sigma}(\chi_\sigma) \frac{D_\sigma}{\tau_\sigma} \varepsilon_{C\sigma\sigma}^{\text{UEG}} d\mathbf{r}. \quad (7)$$

The D_σ/τ_σ ratio is plotted along the internuclear coordinate of the argon dimer in Fig. 3. This plot also shows atomic shell structure, but the choice of denominator ensures that the ratio approaches zero asymptotically for all atoms. From the figure, it can also be seen that D_σ/τ_σ has much less variation than $D_\sigma/D_\sigma^{\text{UEG}}$ at the argon dimer midpoint. Indeed, $D_\sigma/\tau_\sigma=1$ at the dimer midpoint. This explains the reduced grid size dependence in the M05 and M05-2X PESs compared to B1B95 (see Fig. 1). Nevertheless, M05 and M05-2X still produce oscillating potentials with smaller (default) grids. With sparse grids, such as the default grid used in the Gaussian program, uneven sampling of the midpoint region still yields energy oscillations as the complex is stretched.

The TPSS exchange and correlation functionals both depend on the kinetic-energy density, through the ratio $\tau_\sigma^W/\tau_\sigma$. That is, the form of the TPSS exchange functional is

$$E_X^{\text{TPSS}} = \sum_\sigma \int f_{X\sigma} \left(\chi_\sigma^2 \frac{\tau_\sigma^W}{\tau_\sigma} \right) \varepsilon_X^{\text{UEG}} d\mathbf{r}. \quad (8)$$

The TPSS correlation functional has a more complex form, but is also dependent on $\tau_\sigma^W/\tau_\sigma$. The values of this ratio along the argon-argon internuclear axis are also shown in Fig. 3. Like ELF, the $\tau_\sigma^W/\tau_\sigma$ ratio is also a good indicator of atomic shell structure,⁴⁰ and the plot in Fig. 3 reflects this. The curve shows a small dip where τ_σ^W is zero at the dimer midpoint. While the sensitivity to grid sparseness in the correlation energies should be much smaller with TPSS than with B1B95, the TPSS exchange energies are also dependent on $\tau_\sigma^W/\tau_\sigma$. This is potentially significant since exchange energies are much larger than correlation energies. For the argon dimer, the TPSS potential is smooth with the ultrafine grids, but displays barely noticeable oscillations with the default grid. The PES for the benzene dimer (Fig. 2) shows a few barely noticeable “kinks,” as seen for GGA and hybrid-GGA functionals with default grids.¹

The kinetic-energy dependence of the BMK functional is limited to the exchange part,

$$E_X^{\text{BMK}} = \sum_\sigma \int [g_{X\sigma,t}(\chi_\sigma^2) + f_{X\sigma}(w_\sigma)g_{X\sigma,n-t}(\chi_\sigma^2)] \varepsilon_X^{\text{UEG}} d\mathbf{r}. \quad (9)$$

The τ -dependence comes from

$$w_\sigma = \frac{D_\sigma^{\text{UEG}} - \tau_\sigma}{D_\sigma^{\text{UEG}} + \tau_\sigma}, \quad (10)$$

as well as its third and fifth powers in the $f_{X\sigma}(w_\sigma)$ function of the integrand. w_σ approaches -1 in the limit of $\rho_\sigma \rightarrow 0$, as occurs at the argon dimer midpoint. The behavior of w_σ is also shown in Fig. 3. This is the only curve that does not have a peak or dip at the midpoint, and thus we expect BMK to give PESs with no oscillation and similar grid sensitivity as GGA functionals, as is the case in Figs. 1 and 2.

Finally we consider VSXC and the M06-type functionals. For these methods, the oscillations are again entirely due

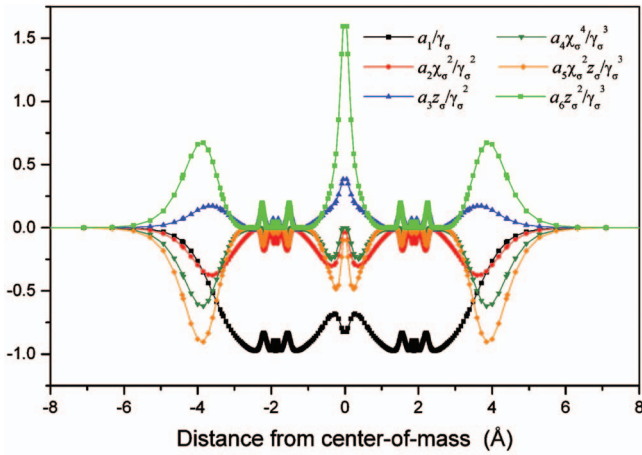


FIG. 4. Plot of the τ -dependent terms in the integrand of the VSXC exchange functional at grid points along the internuclear coordinate of argon dimer, at its experimental equilibrium geometry ($R=3.76$ Å). The results were obtained from post-LSDA calculations (Ref. 36) using 160 radial grid points per atom, and are given in atomic units.

to the τ -dependent terms. While there are differences in the overall functional forms, the τ -dependent terms are the same for VSXC and all the M06-type functionals, except for the values of the empirical parameters a_1 – a_6 in the following equations. The kinetic-energy density is present in more terms in the VSXC functional than in the other meta-GGAs. The VSXC exchange functional is

$$E_X^{\text{VSXC}} = \sum \int f_{X\sigma}(\chi_\sigma, z_\sigma) \epsilon_X^{\text{UEG}} d\mathbf{r}, \quad (11)$$

where the τ -dependence comes from the factor

$$f_{X\sigma}(\chi_\sigma, z_\sigma) = \frac{a_1}{\gamma_\sigma(\chi_\sigma, z_\sigma)} + \frac{a_2\chi_\sigma^2 + a_3z_\sigma}{\gamma_\sigma^2(\chi_\sigma, z_\sigma)} + \frac{a_4\chi_\sigma^4 + a_5\chi_\sigma^2z_\sigma + a_6z_\sigma^2}{\gamma_\sigma^3(\chi_\sigma, z_\sigma)}. \quad (12)$$

In this equation,

$$\gamma(\chi_\sigma, z_\sigma) = 1 + a_7(\chi_\sigma^2 + z_\sigma), \quad (13)$$

the a_i 's are empirical fit parameters, and

$$z_\sigma = \frac{\tau_\sigma}{\rho_\sigma^{5/3}} - \frac{3}{5}(6\pi^2)^{2/3}. \quad (14)$$

The correlation terms have very similar forms, with

$$E_{C\alpha\beta}^{\text{VSXC}} = \int f_{C\alpha\beta}(\chi_{\alpha\beta}, z_{\alpha\beta}) \epsilon_{C\alpha\beta}^{\text{UEG}} d\mathbf{r}, \quad (15)$$

$$E_{C\sigma\sigma}^{\text{VSXC}} = \int f_{C\sigma\sigma}(\chi_\sigma, z_\sigma) D_\sigma \epsilon_{C\sigma\sigma}^{\text{UEG}} d\mathbf{r}, \quad (16)$$

where $\chi_{\alpha\beta}^2 = \chi_\alpha^2 + \chi_\beta^2$ and $z_{\alpha\beta} = z_\alpha + z_\beta$.

The behavior of the τ -dependent terms in the integrand of the VSXC exchange functional along the argon dimer internuclear axis are shown separately in Fig. 4. The correlation terms are not shown, but they should give similar curves. The figure shows that the last (a_6) term in Eq. (12)

has the greatest divergence at the midpoint, but the other terms also change rapidly near the midpoint and will be sensitive to integration grid sparseness.

This sheds light on the differences between the PESs obtained with VSXC and the various M06-type functionals. All of the terms in Eq. (12) are included in VSXC, but in development of the M06-L functional, the a_6 parameter was set to zero for exchange, opposite-, and parallel-spin correlation in an attempt to eliminate oscillations in the dispersion binding curves.²¹ This accounts for the reduced magnitude of the oscillations in the M06-L potentials compared to VSXC. The values of the a_6 parameter for exchange and correlation are also zeroed for the other M06-type functionals. In M06 and M06-HF, the a_4 and a_5 parameters are additionally set to zero for the exchange terms only.^{15,25} Since the variations in these terms at dimer midpoints are no more pronounced than for the first three in Eq. (12), this does not noticeably decrease the oscillations in the PESs, relative to M06-L. Finally, in M06-2X, the coefficients of all the τ -dependent exchange terms of Eq. (12) are set to zero.¹⁵ Some sensitivity to integration grid sparseness is still expected from the M06-2X correlation functional. However, since correlation energies are much smaller than exchange energies, any oscillations should have much smaller amplitudes. This explains why the M06-2X curves appear smooth with ultrafine or finer integration grids, while all the other M06-type functionals give oscillatory PESs.

IV. SUMMARY AND CONCLUSIONS

The integrands of GGA exchange-correlation functionals depend on the dimensionless (“reduced”) gradient variable $|\nabla\rho|/\rho^{4/3}$ which approaches zero at the intermonomer midpoint in any dispersion-bound complex. Reduced variables in meta-GGAs, however, may take many forms. Common forms include $D_\sigma/D_\sigma^{\text{UEG}}$, D_σ/τ_σ , $\tau_\sigma^w/\tau_\sigma$, and $w_\sigma = (D_\sigma^{\text{UEG}} - \tau_\sigma)/(D_\sigma^{\text{UEG}} + \tau_\sigma)$.

All of these, except w_σ , vary markedly near intermonomer midpoints, displaying a pronounced rise (a near divergence in the case of $D_\sigma/D_\sigma^{\text{UEG}}$) or pronounced dip. Unless midpoint regions in dispersion-bound complexes are very well sampled by integration grids, the resulting meta-GGA PESs are prone to spurious oscillations and other random noise. Spurious oscillations are evident (see Figs. 1 and 2) in most meta-GGAs when standard grids are employed.

Users of meta-GGAs should be aware of this problem, and designers of meta-GGAs should attempt to avoid it. Also, we reiterate in this work that meta-GGAs, just as GGAs, do not incorporate the physics of dispersion correlations and should not be expected to well represent dispersion-dominated PESs. Dispersion physics must be explicitly built into density-functional theories for reliable treatment of weakly interacting systems.^{10–13}

ACKNOWLEDGMENTS

This work was supported by the Natural Sciences and Engineering Research Council of Canada, the Atlantic

Computing Excellence Network, the Killam Trust of Dalhousie University, and the National Science Foundation (Grant No. CHE-0715268).

- ¹E. R. Johnson, R. A. Wolkow, and G. A. DiLabio, *Chem. Phys. Lett.* **394**, 334 (2004).
- ²A. J. Stone, *The Theory of Intermolecular Forces* (Clarendon, Oxford, 1996).
- ³J. M. Pérez-Jordá and A. D. Becke, *Chem. Phys. Lett.* **233**, 134 (1995).
- ⁴Y. Zhang, W. Pan, and W. Yang, *J. Chem. Phys.* **107**, 7921 (1997).
- ⁵F. O. Kannemann and A. D. Becke, *J. Chem. Theory Comput.* **5**, 719 (2009).
- ⁶S. D. Chao and A. H.-T. Li, *J. Phys. Chem. A* **111**, 9586 (2007).
- ⁷A. D. Becke, *Phys. Rev. A* **38**, 3098 (1988).
- ⁸J. P. Perdew, K. Burke, and M. Ernzerhof, *Phys. Rev. Lett.* **77**, 3865 (1996).
- ⁹M. J. Allen and D. J. Tozer, *J. Chem. Phys.* **117**, 11113 (2002).
- ¹⁰A. D. Becke and E. R. Johnson, *J. Chem. Phys.* **127**, 124108 (2007); **127**, 154108 (2007).
- ¹¹Y. Andersson, D. C. Langreth, and B. I. Lundqvist, *Phys. Rev. Lett.* **76**, 102 (1996); T. Sato, T. Tsuneda, and K. Hirao, *J. Chem. Phys.* **123**, 104307 (2005); M. Dion, H. Rydberg, E. Schröder, D. C. Langreth, and B. I. Lundqvist, *Phys. Rev. Lett.* **92**, 246401 (2004); **95**, 109902 (2005); O. A. Vydrov, Q. Wu, and T. Van Voorhis, *J. Chem. Phys.* **129**, 014106 (2008).
- ¹²Q. Wu and W. Yang, *J. Chem. Phys.* **116**, 515 (2002); S. Grimme, *J. Comput. Chem.* **25**, 1463 (2004); S. Grimme, *ibid.* **27**, 1787 (2006); J. Antony and S. Grimme, *Phys. Chem. Chem. Phys.* **8**, 5287 (2006); R. Jurecka, J. Cerny, P. Hobza, and D. R. Salahub, *J. Comput. Chem.* **28**, 555 (2007).
- ¹³G. A. DiLabio, *Chem. Phys. Lett.* **455**, 348 (2008); I. D. Mackie and G. A. DiLabio, *J. Phys. Chem. A* **112**, 10968 (2008).
- ¹⁴J. Tao and J. P. Perdew, *J. Chem. Phys.* **122**, 114102 (2005); A. Ruzsinszky and J. P. Perdew, *J. Phys. Chem. A* **109**, 11015 (2005).
- ¹⁵Y. Zhao and D. G. Truhlar, *Theor. Chem. Acc.* **120**, 215 (2008).
- ¹⁶A. D. Becke, *J. Chem. Phys.* **112**, 4020 (2000).
- ¹⁷J. Tao, J. P. Perdew, V. N. Staroverov, and G. E. Scuseria, *Phys. Rev. Lett.* **91**, 146401 (2003).
- ¹⁸T. Van Voorhis and G. E. Scuseria, *J. Chem. Phys.* **109**, 400 (1998); **129**, 219901 (2008).
- ¹⁹A. D. Becke, *J. Chem. Phys.* **104**, 1040 (1996).
- ²⁰A. D. Becke, *J. Chem. Phys.* **98**, 5648 (1993).
- ²¹Y. Zhao and D. G. Truhlar, *J. Chem. Phys.* **125**, 125 (2006).
- ²²C. A. Jiménez-Hoyos, B. G. Janesko, and G. E. Scuseria, *Phys. Chem. Chem. Phys.* **10**, 6621 (2008).
- ²³A. D. Boese and J. M. L. Martin, *J. Chem. Phys.* **121**, 3405 (2004).
- ²⁴Y. Zhao, N. E. Schultz, and D. G. Truhlar, *J. Chem. Theory Comput.* **2**, 364 (2006).
- ²⁵Y. Zhao and D. G. Truhlar, *J. Phys. Chem. A* **110**, 13126 (2006).
- ²⁶M. J. Frisch, G. W. Trucks, H. B. Schlegel *et al.*, GAUSSIAN03, Revision D.01, Gaussian, Inc., Wallingford, CT, 2004.
- ²⁷E. J. Bylaska, W. A. de Jong, N. Govind *et al.*, NWChem, A Computational Chemistry Package for Parallel Computers, Version 5.1, Pacific Northwest National Laboratory, Richland, WA, 2007. A modified version.
- ²⁸C. D. Sherrill, T. Takatani, and E. G. Hohenstein, *J. Phys. Chem. A* (in press).
- ²⁹R. E. Stratmann, G. Scuseria, and M. J. Frisch, *Chem. Phys. Lett.* **257**, 213 (1996).
- ³⁰K. T. Tang and J. P. Toennies, *J. Chem. Phys.* **118**, 4976 (2003).
- ³¹D. J. Lacks and R. G. Gordon, *Phys. Rev. A* **47**, 4681 (1993).
- ³²A. D. Becke, *J. Chem. Phys.* **107**, 8554 (1997).
- ³³F. A. Hamprecht, A. J. Cohen, D. J. Tozer, and N. C. Handy, *J. Chem. Phys.* **109**, 6264 (1998).
- ³⁴J. P. Perdew, J. Tao, V. N. Staroverov, and G. E. Scuseria, *J. Chem. Phys.* **120**, 6898 (2004); J. Gräfenstein, D. Izotov, and D. Cremer, *ibid.* **127**, 214103 (2007).
- ³⁵H. Stoll, C. M. E. Pavlidou, and H. Preuss, *Theor. Chim. Acta* **49**, 143 (1978); H. Stoll, E. Golka, and H. Preuss, *ibid.* **55**, 29 (1980).
- ³⁶A. D. Becke, *Int. J. Quantum Chem., Symp.* **23**, 599 (1989); A. D. Becke and R. M. Dickson, *J. Chem. Phys.* **92**, 3610 (1990).
- ³⁷J. P. Perdew and Y. Wang, *Phys. Rev. B* **45**, 13244 (1992).
- ³⁸A. D. Becke and K. E. Edgecombe, *J. Chem. Phys.* **92**, 5397 (1990).
- ³⁹A. D. Becke, *J. Chem. Phys.* **109**, 2092 (1998).
- ⁴⁰H. L. Schmider and A. D. Becke, *J. Mol. Struct.: THEOCHEM* **527**, 51 (2000).